RESEARCH PAPER

COACTION PUBLISHING

Broad segmental progeroid changes in short-lived *Ercc1*$^{-/\Delta 7}$ mice

Martijn E.T. Dollé[1]*, Raoul V. Kuiper[2], Marianne Roodbergen[1], Joke Robinson[1], Sisca de Vlugt[1], Susan W.P. Wijnhoven[1], Rudolf B. Beems[1], Liset de la Fonteyne[1], Piet de With[1], Ingrid van der Pluijm[3], Laura J. Niedernhofer[4], Paul Hasty[5], Jan Vijg[6], Jan H.J. Hoeijmakers[3] and Harry van Steeg[1]

[1]Laboratory of Heath Protection Research, National Institute of Public Health and the Environment, Bilthoven, The Netherlands; [2]Pathobiology Department, Dutch Molecular Pathology Center, Faculty of Veterinary Medicine, Utrecht University, Utrecht, The Netherlands; [3]Medical Genetic Center-Department of Cell Biology and Genetics, Center for Biomedical Genetics, Erasmus Medical Center, Rotterdam, The Netherlands; [4]Department of Microbiology and Molecular Genetics, University of Pittsburgh School of Medicine, Pittsburgh, PA, USA; [5]The Department of Molecular Medicine, The University of Texas Health Science Center at San Antonio, The Institute of Biotechnology, San Antonio, TX, USA; [6]Departments of Genetics, Ophthalmology & Visual Sciences and Obstetrics & Gynecology and Women's Health, Albert Einstein College of Medicine, Bronx, NY, USA

Genome maintenance is considered a prime longevity assurance mechanism as apparent from many progeroid human syndromes that are caused by genome maintenance defects. The ERCC1 protein is involved in three genome maintenance systems: nucleotide excision repair, interstrand cross-link repair, and homologous recombination. Here we describe in-life and post-mortem observations for a hypomorphic *Ercc1* variant, *Ercc1*$^{-/\Delta 7}$, which is hemizygous for a single truncated *Ercc1* allele, encoding a protein lacking the last seven amino acids. *Ercc1*$^{-/\Delta 7}$ mice were much smaller and median life span was markedly reduced compared to wild-type siblings: 20 and 118 weeks, respectively. Multiple signs and symptoms of aging were found to occur at an accelerated rate in the *Ercc1*$^{-/\Delta 7}$ mice as compared to wild-type controls, including a decline in weight of both whole body and various organs, numerous histopathological lesions, and immune parameters. Together they define a segmental progeroid phenotype of the *Ercc1*$^{-/\Delta 7}$ mouse model.

Keywords: *Ercc1*; *mouse*; *aging*; *life span*; *cross sectional*; *pathology*; *immunosenescense*; *body weight*; *organ weight*; *FVB*; *C57BL/6*; *genome maintenance*

Received: 20 April 2011; Revised: 17 May 2011; Accepted: 17 May 2011; Published: 1 June 2011

Genome maintenance is often considered a longevity-assurance system, i.e. one of the mechanisms to preserve the integrity of cells and tissues necessary for living out a genetically pre-determined, normal life span. Genome maintenance is critically important for the uninterrupted translation of the genomic code into function and the preservation of cell viability. Deficiencies in genome maintenance proteins can result in reduced life span and segmental progeroid pathology (1, 2).

Though several classes of genome maintenance mechanisms exist, a key cluster is formed by DNA repair pathways, removing DNA lesions caused by both endogenous and exogenous sources. One such DNA repair pathway is nucleotide excision repair (NER), removing a broad spectrum of helix-distorting lesions ranging from UV-induced DNA damage and numerous bulky chemical adducts to several types of oxidative damages produced by endogenous metabolism, as to resolve transcription obstructions and to reduce mutagenic errors prior to DNA duplication. NER comprises the concerted action of over 30 gene products. Two subpathways are recognized differing in damage recognition but sharing the same core repair machinery: global genome repair for the removal of distorting lesions anywhere in the genome and transcription-coupled repair for the elimination of distorting DNA damage that blocks transcription. Previously we have shown that disabling NER in mice can

 Citation: Pathobiology of Aging & Age-related Diseases 2011, **1**: 7219 - DOI: 10.3402/pba.v1i0.7219

lead to different phenotypes depending on the protein compromised and resembling the phenotypic features of the corresponding human syndrome. For example, *Xpa* and *Xpc* null mice, defective for proteins involved in damage verification and global damage recognition steps, respectively, only show a tumor phenotype and a reduced life span, thereby mimicking the human xeroderma pigmentosum (XP) phenotype (3). On the other hand, *Xpd* mutant mice, defective for one of two helicases of the transcription and NER factor TFIIH and modeled after a mutation of a Trichothiodystrophy (TTD) patient, show other segmental aging characteristics such as femoral osteoporosis, renal anisokaryosis, hepatic lipofuscin accumulation, and a reduced life span. Remarkably, TTD mice also showed signs of delayed aging resembling features commonly observed in diet-restricted mice including decreased fat depots, diminished eye lens cataracts, reduced thyroid follicular distension, and reduced tumor incidence (4).

In this report we describe the aging-associated pathology of yet another DNA repair compromised mutant mouse model, *Ercc1*. Together with XPF, ERCC1 forms an endonuclease required for incising the damaged strand of DNA in NER 5′ to the lesion. In addition, the nuclease heterodimer is required to resolve DNA interstrand cross-links (5) and has a role in subpathways of homologous recombination repair (6). Hence, Ercc1 deficient mice are compromised in multiple DNA repair pathways evidenced by their sensitivity to UV, ionizing radiation and alkylating and cross-linking agents (6–8). Ercc1 deficiency has been modeled as two genetic variants in mice: a complete knock out ($Ercc1^{-/-}$) and a mutation deleting the last seven amino acids at the C-terminus of the wild-type protein ($Ercc1^{\Delta 7/\Delta 7}$) (7). Many explicit phenotypes have been reported for the severely runted and extremely short-lived $Ercc1^{-/-}$ mouse model, including hepatic and renal nuclear abnormalities and reduced hematopoetic reserves (9–11). Here we use the hybrid genotype of the null and the seven amino acid deletion ($Ercc1^{-/\Delta 7}$). In contrast to the full knock-out, this hybrid genotype results in a phenotype that lives several weeks beyond weaning age and accumulates genomic mutations at increased frequencies compared to same-age wild-type siblings (12). We show that the short lived $Ercc1^{-/\Delta 7}$ mice develop a broad spectrum of aging-related changes also observed in wild-type mice, but with varying rates between lesions.

Materials and methods

Mice

Heterozygous $Ercc1^{+/-}$ knockout mice (7) and heterozygous *pUR288(lacZ)* transgenic line 30 mice (12) were each backcrossed for more than 10 generations to C57BL6/JIco mice (Charles River, France). In parallel, heterozygous $Ercc1^{+/\Delta 7}$ mutant mice, carrying a deletion removing the last seven amino acids at the C-terminus of the wild-type protein (7), were backcrossed for more than 10 generations to FVB/NHan^{TM}Hsd mice (Harlan, Germany). Subsequently, to offer the possibility to monitor genomic instability (12), the $Ercc1^{+/-}$ C57BL/6J mice and *pUR288(lacZ)* C57BL/6J mice were crossbred to generate $Ercc1^{+/-}$ mice homozygous for the *pUR288(lacZ)*-transgene in a C57BL/6J background. In combination with the $Ercc1^{+/\Delta 7}$ FVB mice these $Ercc1^{+/-}$, $pUR288^{+/+}$ C57BL/6 mice formed the breeding pairs to directly generate both wild-type $Ercc1^{+/+}$, $pUR288^{+/-}$ control and $Ercc1^{-/\Delta 7}$, $pUR288^{+/-}$ repair deficient mice in a hybrid C57BL/6-FVB F1-background as sib-pairs. Heterozygous $Ercc1^{+/-}$ or $Ercc1^{+/\Delta 7}$ siblings were discarded.

Genotyping was performed on DNA isolated from tail tips. *Ercc1* alleles were genotyped by PCR coamplification of various regions: the exon-7-sense and exon-8-antisense primer combination produces a 780 bp fragment for the wild-type or the mutant (delta 7) allele; the *neo^r*-sense and exon-8-antisense primer combination produces a 880 bp fragment specific for the null allele; and the *neo^r*-sense and 3′-UTR-antisense primer combination produces a 600 bp fragment specific for the mutant allele (exon-7-sense: 5′-GAAAAGCTGGAGCAGAACTT, exon-8-antisense: 5′-AGATTTCACGGTGGTCAGAC, *neo^r*-sense: 5′-GA AGAGCTTGGCGGCGAATG, and 3′-UTR-antisense: 5′-TATTGTGACATGGGCCTAGGTGGCA). The amplified fragments were size separated on a 1.5% agarose gel. The presence of the pUR288 transgenic reporter allele was performed by a separate PCR reaction as described previously (13).

All breeding and cohort housing were done under specific pathogen-free (SPF) conditions, monitored every 3 months. Except for *Citrobacter rodentium*, SPF screening included all FELASA suggested mouse pathogens (14) and six additional viruses (Hanta, K-, Killhamrat, Parainfluenza 3, Polyoma, and Simian virus 5). No infections were detected. After weaning, all mice were housed in groups of four or less by genotype and sex at 20°C with a light/dark cycle of 12 hr/12 hr. The CRM pelleted breeder and maintenance diet, 25kGy irradiated (Special Diet Services, UK), and water were supplied *ad libitum*. All mice showing moribund conditions prior to their natural death or cross-sectional kill date were euthanized. Moribund conditions were specified as >15% weight loss within 2 weeks, prominent appearing ribs and spine and sunken hips, hunched body position with matted fur, not responsive to touch, slow respiration, rectal or uterine prolapse, prominent skin lesions, or a visible tumor. Euthanasia of moribund or cross-sectional animals was performed by intramuscular injection of a Ketamine–Rompun mixture, followed by exsanguination. All experiments were performed in

Citation: Pathobiology of Aging & Age-related Diseases 2011, **1**: 7219 - DOI: 10.3402/pba.v1i0.7219

accordance with all applicable federal and institutional policies.

Experimental design

Initially, life span cohorts were generated comprising 31 male and 29 female *Ercc1*$^{-/\Delta 7}$, *pUR288*$^{+/-}$ and 50 male and 51 female *Ercc1*$^{+/+}$, *pUR288*$^{+/-}$ siblings. Subsequently, animals for the cross-sectional cohorts were generated and randomly allocated to different age groups. For the cross-sectional cohorts, the following age-groups and animal numbers were used for *Ercc1*$^{-/\Delta 7}$: 4 weeks – 15 mice per sex, 10 weeks – 7 mice per sex, 14 weeks – 8 to 10 mice per sex, 16 weeks – 14 mice per sex, and 20 weeks – 16 mice per sex; and for *Ercc1*$^{+/+}$: 4 weeks – 6 to 7 mice per sex, 10 weeks – 6 to 7 mice per sex, 13 weeks – 15 mice per sex, 52 weeks – 15 to 16 mice per sex, and 96 weeks – 17 to 18 mice per sex. Only mice surviving past weaning age (3 weeks) entered the cohort studies; hence, mice dying before 3 weeks of age had no effect on the number of animals in any of the cohorts. Early spontaneous death or moribund appearance beyond 3 weeks of age, but before the scheduled age of death, lowered the effective number of mice available in the cross-sectional cohorts. Supplementary Table 1 provides a summary of fate and animal numbers for each subcohort. Individual live animal weights were measured weekly for *Ercc1*$^{-/\Delta 7}$ and biweekly for *Ercc1*$^{+/+}$ mice. Total body weights as well as various dissected organ weights were determined at time of death. The total body weights were determined before any phlebotomy.

Pathology

Forty-three organs and tissue samples of intact animals were dissected for histopathology (see Supplementary Table 2), and preserved in a neutral aqueous phosphate-buffered, pH 7.0–7.4, 4% w/v (or 10% v/v) solution of formaldehyde (Klinipath, Duiven, the Netherlands). In addition, samples of 20 different organs and tissues were snap-frozen in liquid nitrogen (Supplementary Table 2) for further molecular biological analysis (to be published elsewhere). Tissues required for microscopic examination were embedded in paraffin wax, sectioned at 4 µm and stained with haematoxylin and eosin (H&E). Furthermore, unstained liver slides were prepared for lipofuscin UV-autofluorescence determination (15).

Scores of all lesions ranged from 0 to 5 (0 = absent, 1 = minimal, 2 = slight, 3 = moderate, 4 = severe, 5 = very severe). These scores were 'absolute' and not relative to the severity in wild-type mice. In case of doubt, a blind and random examination of the slides was performed to provide an objective assessment of the severity.

Flow cytometric analysis

Single-cell suspensions from mouse spleen and thymus halves were prepared immediately after autopsy, followed by the determination of lymphocyte subset distributions, which were performed essentially as described before (16). Combinations of the following antibodies were used: FITC hamster-anti-mouse CD3e, PE rat-anti-mouse CD8a, FITC rat-anti-mouse CD8a, PerCP^{TM}5.5 rat-anti-mouse CD4, PerCP^{TM}5.5 rat-anti-mouse CD45, PE rat-anti-mouse CD45R/B220, APC mouse-anti-mouse NK-1.1, PE rat-anti-mouse CD45RB, and APC rat-anti-mouse CD44 (Pharmingen, San Diego, CA)

Statistical analyses

Life span curves were compared in pairs using the logrank test in Prism 4.03 (GraphPad Software). Pathology scores between two groups were compared using the two-tailed Mann–Whitney test.

Lipofuscin histopathology scores were analyzed using the PROAST software v22.5 (www.rivm.nl/proast) (17), where the scores are treated as ordinal data. These discrete scores can be interpreted as reflecting particular consecutive ranges in the level of lipofuscin, which is in reality a continuous variable. In PROAST a so-called latent variable model can be fitted to this type of data, by fitting an exponential model to the underlying continuous variable, while at the same time estimating the boundaries in that continuous variable that demarcate the consecutive ranges indicated by the observed scores. The exponential model can be regarded as a nested family of models, which allows for an analysis where the number parameters in the model for describing the particular data is determined by applying a likelihood ratio test, as described by Slob (17). After fitting the model, the expected time point for a mouse in a particular genotype/age group to reach a respective pathology score is estimated from the fitted model, with a (two-sided) 90% confidence interval.

Results

Life span

Two *Ercc1* cohort studies were conducted: one life span study and one cross-sectional study. Both *Ercc1*-deficient and wild-type siblings for both cohorts were generated as C57BL/6-FVB F1 hybrid mice by cross-breeding C57BL/6 *Ercc1*$^{+/-}$ mice with FVB, *Ercc1*$^{+/\Delta 7}$ mice. At 2 weeks of age, all mice were genotyped: 16% had the *Ercc1*$^{-/\Delta 7}$ genotype; 56% of the *Ercc1*$^{-/\Delta 7}$ mice survived past weaning age of 3 weeks after which they entered the life span and cross-sectional cohorts. The life span cohorts are based on 31 male and 29 female *Ercc1*$^{-/\Delta 7}$ and 50 male and 51 female *Ercc1*$^{+/+}$ wild-type siblings. The resulting life span curves (Fig. 1A) show a median life span and maximal life span of 19 and 26 weeks for male and 21 and 29 weeks for female *Ercc1*$^{/\Delta 7}$ mice, respectively. Logrank testing indicated a significant (p = 0.0406) difference in life span between the two sexes of

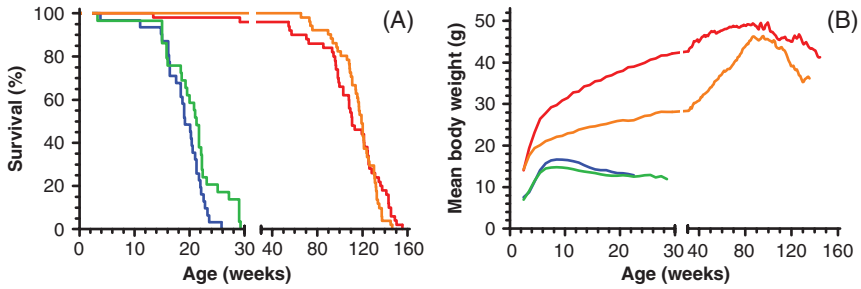

Fig. 1. Life span (A) and mean body weight (B) curves of *Ercc1*$^{-/\Delta 7}$ and *Ercc1*$^{+/+}$ sibling control mice of the life span cohorts. Mice entered the study at weaning age (3 weeks); deaths before weaning age are not depicted (see text). *Ercc1*$^{-/\Delta 7}$ males: blue ($n=31$); *Ercc1*$^{-/\Delta 7}$ females: green ($n=29$); *Ercc1*$^{+/+}$ males: red ($n=50$); and *Ercc1*$^{+/+}$ females: orange ($n=51$).

Ercc1$^{-/\Delta 7}$ mice. Their wild-type siblings lived almost six times as long ($p<0.0001$) with a median life span and maximum life span of 111 and 156 weeks for male and 119 and 146 weeks for female *Ercc1*$^{+/+}$ mice, respectively. There was no significant difference in life span between male and female *Ercc1*$^{+/+}$ mice.

Body weights

Besides a reduced life span, *Ercc1*$^{-/\Delta 7}$ mice have a runted phenotype already discernible at birth and exemplified by their mean body weight curves depicted in Fig. 1B. Both male and female *Ercc1*$^{-/\Delta 7}$ mice reach their maximum mean body weights of 16.7 and 14.8 g, respectively, at 8- to 9-weeks of age, after which the mean body weights gradually decline. In contrast *Ercc1*$^{+/+}$ mice have reached mean body weights of 29.8 g (males) and 21.1 g (females) at that young age. Subsequently, female *Ercc1*$^{+/+}$ show a rather linear increase of mean body weight to a maximum of 46.3 g at 87 weeks of age, whereas males display a more logarithmic increase, reaching a maximum mean of 49.4 g at 87 weeks. Beyond 90 weeks of age mean body weights of both male and female wild-type mice declined gradually. The longitudinal body weight data of the life span cohorts was confirmed by the body weights of the cross-sectional cohort (Fig. 2A). The average weight at time of death of moribund animals of the life span cohorts was 12.0 ± 1.6 for male and 11.6 ± 1.1 for female *Ercc1*$^{-/\Delta 7}$ mice and 39 ± 6 g for male and 35 ± 9 g for female *Ercc1*$^{+/+}$ mice (Fig. 2A). Inspection of the oral cavity showed no abnormalities. Moreover, food consumption by *Ercc1*$^{-/\Delta 7}$ mice expressed per gram body weight was about 1.3 times higher than their *Ercc1*$^{+/+}$ siblings (results not shown), indicating that the severely reduced body weight development of *Ercc1*$^{-/\Delta 7}$ mice was not due to hindered food intake.

Organ weights

Organ weights were determined at the scheduled interim sacrifices of the cross-sectional cohorts, as these weights give a good impression of the trends in organ weights in relatively healthy animals at their chronological age groups. In contrast, the organ weights of euthanized animals of the life span cohorts relate to moribund conditions, and were grouped as a biological age group termed 'end-of-life'. The mean total body and mean absolute organ weights of the cross-sectional cohorts and the end-of-life time point of the life span cohorts are displayed in Fig. 2. Liver (Fig. 2D) and heart (Fig. 2H) weight development follows the weight development of the total body weight for both genotypes. These organs have a rather constant relative organ weight over the entire life span, making up about 6% for liver (Fig. 2E) and 0.6% for heart (Fig. 2I) relative to total body weight.

Whereas in *Ercc1*$^{+/+}$ animals, kidney weights follow the same body weight related trend (Fig. 2C) as liver and heart, kidney weights in *Ercc1*$^{-/\Delta 7}$ animals show a minimal age-related decline in absolute organ weight after 10 weeks of age (Fig. 2B). The decline in total body weight after 10 weeks of age, results in an increase of relative kidney weight after that age for *Ercc1*$^{-/\Delta 7}$ mice, particularly for males (Fig. 2C).

Absolute spleen weights (Fig. 2F) remain constant in *Ercc1*$^{+/+}$ mice, at least up until middle age (52 weeks). In the oldest cross-sectional group (96 weeks) and in the end-of-life group about half of the *Ercc1*$^{+/+}$ females had enlarged spleens, most of which were affected by lymphoma or myeloid leukemia. The absolute spleen weights decreased in *Ercc1*$^{-/\Delta 7}$ after 10 weeks of age.

Absolute thymus weights decline with age in all genotypes (Fig. 2J). The relative thymus weights decrease from about 0.45% of total body weight at 4 weeks of age to about 0.05% in the oldest and the end-of-life groups for all genotypes (Fig. 2K). Chronologically thymic involution in *Ercc1*$^{-/\Delta 7}$ mice is accelerated compared to their *Ercc1*$^{+/+}$ siblings. However, on a biological time scale thymic involution rates appear similar between the two genotypes.

After initial growth during development the absolute brain weight in *Ercc1*$^{+/+}$ mice shows a very modest increase from age 10 weeks until old age (Fig. 2L). In contrast *Ercc1*$^{-/\Delta 7}$ mice lose brain mass after 10 weeks of age. The age related brain weight reduction coincides with the ataxic phenotype that these mice start to develop at

Citation: Pathobiology of Aging & Age-related Diseases 2011, **1**: 7219 - DOI: 10.3402/pba.v1i0.7219

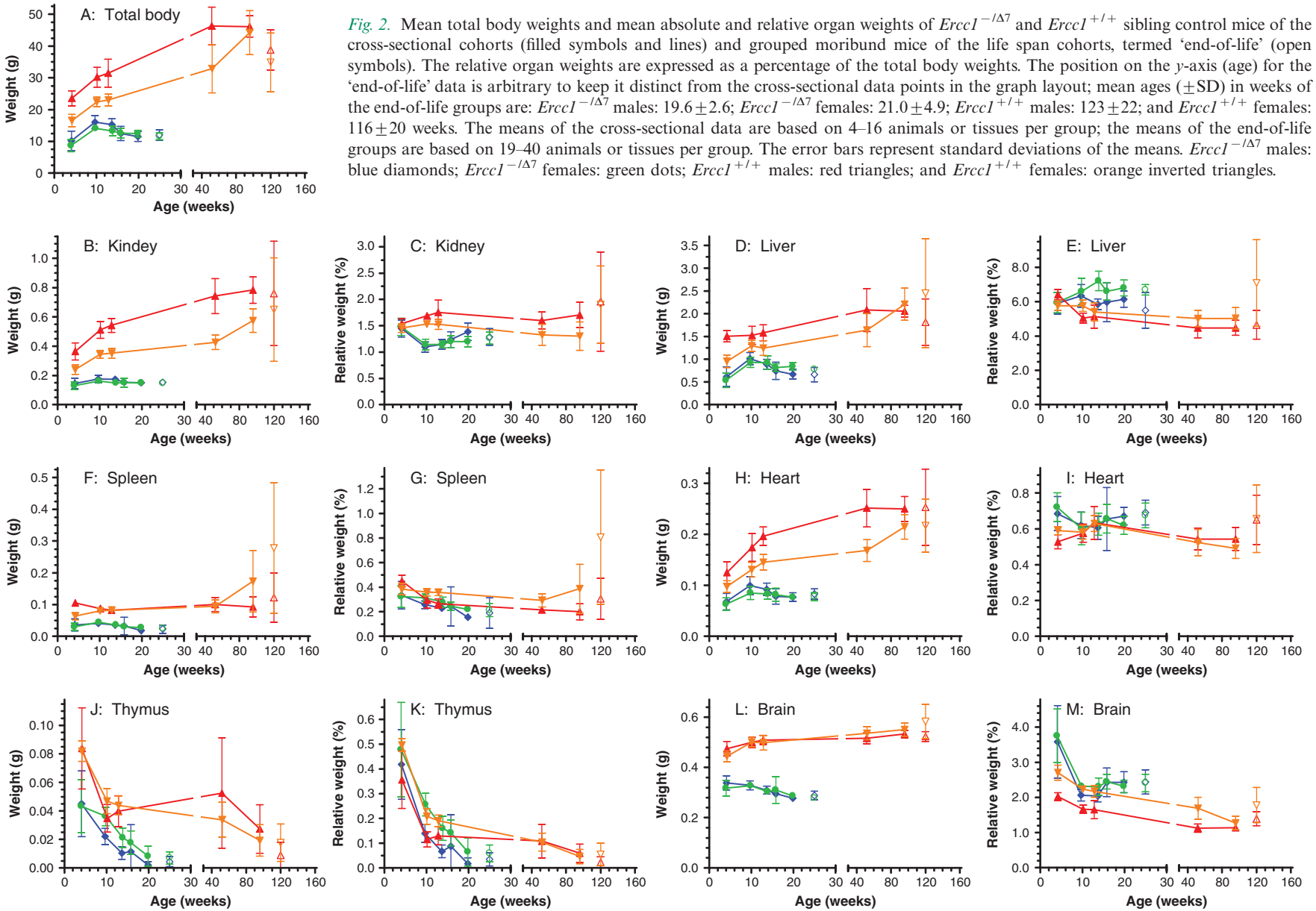

Fig. 2. Mean total body weights and mean absolute and relative organ weights of *Ercc1*$^{-/\Delta 7}$ and *Ercc1*$^{+/+}$ sibling control mice of the cross-sectional cohorts (filled symbols and lines) and grouped moribund mice of the life span cohorts, termed 'end-of-life' (open symbols). The relative organ weights are expressed as a percentage of the total body weights. The position on the *y*-axis (age) for the 'end-of-life' data is arbitrary to keep it distinct from the cross-sectional data points in the graph layout; mean ages (±SD) in weeks of the end-of-life groups are: *Ercc1*$^{-/\Delta 7}$ males: 19.6±2.6; *Ercc1*$^{-/\Delta 7}$ females: 21.0±4.9; *Ercc1*$^{+/+}$ males: 123±22; and *Ercc1*$^{+/+}$ females: 116±20 weeks. The means of the cross-sectional data are based on 4–16 animals or tissues per group; the means of the end-of-life groups are based on 19–40 animals or tissues per group. The error bars represent standard deviations of the means. *Ercc1*$^{-/\Delta 7}$ males: blue diamonds; *Ercc1*$^{-/\Delta 7}$ females: green dots; *Ercc1*$^{+/+}$ males: red triangles; and *Ercc1*$^{+/+}$ females: orange inverted triangles.

young age, marked by clasping of the hindlegs when lifted by the tail, and body tremors (18). These signs progress as they age, resulting in an unstable gait (behavioral observations; data not shown).

Pathology

All moribund and cross-sectional animals underwent full necropsy and a representative number of organs were microscopically analyzed. Characteristic lesions found in the end-of-life animals of the life span cohorts, were subsequently examined in the cross-sectional cohorts. Despite severe pathological findings in many organs of the *Ercc1*$^{-/\Delta 7}$ mice, a specific set of lesions that would have caused the spontaneous demise of these mice is difficult to assign, and when mice showed significant weight loss they were sacrificed to prevent autolysis after unscheduled death. The marked pathological lesions observed in the life span cohort at end-of-life are summarized in Table 1. Characteristic pathological changes observed in liver and kidney of the cross-sectional cohorts (Fig. 3) exemplify the age-related changes of the histopathological observations in Table 1. In general, sex differences were not detected within genotypes and male and female pathology scores were combined to increase group sizes; exceptions are specifically indicated. Both the end-of-life and age-related observations are described in detail below.

Neoplasia

In contrast to *Ercc1*$^{+/+}$ mice, neoplastic lesions were not observed in any of the analyzed *Ercc1*$^{-/\Delta 7}$ mice. The predominant neoplasms observed in the *Ercc1*$^{+/+}$ animals were from pulmonary, hematopoietic and pituitary origin (results not shown). The tumor spectrum in the hybrid background appears an intermediate of the founder lines, as C57BL/6 mice mainly develop pituitary adenomas and lymphomas, whereas FVB mice have a predisposition for bronchiolo/alveolar tumors (Mouse Tumor Biology Database: http://tumor.informatics.jax.org/mtbwi). In the cross-sectional wild-type cohort tumors were only found in the oldest age group, i.e. 96 weeks of age (results not shown).

Hepatic nuclear morphology and lipofuscin accumulation

Hepatic changes typically observed in aging mice include abnormal nuclear morphology including anisokaryosis (mostly karyomegaly), intranuclear cytoplasmic inclusions, and accumulation of the autofluorescent pigment lipofuscin. Both anisokaryosis and cytoplasmic inclusions are indicative of incomplete cytokinesis, which can occur in aneuploidy or polyploidy, a hallmark in both aging and *Ercc1*$^{-/-}$ mice (7, 9). Although in *Ercc1*$^{+/+}$ mice, anisokaryosis may be observed from the time of weaning, this change is much more severe in *Ercc1*$^{-/\Delta 7}$ (Table 1, Figs. 3C and 4A, B). Intranuclear inclusions are also much more severe and appear at earlier time points than in *Ercc1*$^{+/+}$ (Table 1, Figs. 3D and 4A, B); in *Ercc1*$^{-/\Delta 7}$ they are observed at the earliest age examined (4 weeks). Compared to *Ercc1*$^{-/-}$ mice intranuclear inclusions are more overt in the *Ercc1*$^{-/\Delta 7}$ mice, indicating that this phenotype requires some more time to develop (9, 19).

Lipofuscin is an accumulating autofluorescent pigmented product of lipid and protein metabolism (15) and particularly accumulates in cells of post-mitotic and/or metabolically very active tissues such as brain and liver of aging animals. In the liver, it is most conspicuous in phagocytic Kupffer cells and usually evenly spread over the tissue, which supports reproducible scoring. Liver lipofuscin levels were high at end-of-life in both *Ercc1*$^{-/\Delta 7}$ and *Ercc1*$^{+/+}$ mice (Table 1), even though the *Ercc1*$^{-/\Delta 7}$ mice were much younger in chronological terms. This result was confirmed in cross-sectionally sacrificed animals where lipofuscin accumulation was accelerated in *Ercc1*$^{-/\Delta 7}$ compared to controls (Fig. 3E). Though differences between sexes within genotypes were not detected in the lipofuscin scores at end-of-life (Table 1), statistical modeling of the cross-sectional pathology scores indicated consistent sex differences in liver lipofuscin accumulation rates within genotypes (Fig. 3F), i.e. both *Ercc1*$^{-/\Delta 7}$ and *Ercc1*$^{+/+}$ females showed a faster age-related increase compared to males of the same genotype. The lipofuscin accumulation in brain reflected the findings in the liver (not shown).

Renal nuclear morphology

Abnormally enlarged nuclei of renal tubular epithelial cells (Table 1, Figs. 3A and 4C, D) were particularly noted in *Ercc1*$^{-/\Delta 7}$ mice at all ages. This lesion was also observed in *Ercc1*$^{-/-}$ mice (7, 9) and may represent a signature lesion in Ercc1 deficient mice, as it has not been noted to the same extent even in aged WT mice. Vacuolization of renal tubular epithelium was noted in all animals. Cross-sectional wild-type animals more frequently showed fat vacuoles in their renal tubular epithelium, whereas cloudy swelling (hydropic degeneration) was minimal, but more often observed in *Ercc1*$^{-/\Delta 7}$ mutants; also, the renal cortex was thinner in these animals and tubules were occasionally lined by stretched, attenuated epithelial cells, indicating cell loss and atrophy of the renal cortex. Therefore, loss of degenerating cells in *Ercc1*$^{-/\Delta 7}$ mutants prevented these animals from reaching similar numbers of vacuolated cells as wild-type kidneys (Figs. 3B and 4C, D).

Lymphoid depletion

Ercc1$^{-/\Delta 7}$ mice consistently showed bone marrow loss and replacement by adipocyte invasion (fatty atrophy) over the entire length of the tibia and distal femur

Citation: Pathobiology of Aging & Age-related Diseases 2011, **1**: 7219 - DOI: 10.3402/pba.v1i0.7219

Table 1. Mean histopathology score at end-of-life

	Ercc1$^{+/+}$		*Ercc1*$^{-/\Delta 7}$		
	Mean	95% CI	Mean	95% CI	*p*-Value[a]
Liver anisokaryosis	3.8	(3.3–4.3)	4.1	(3.8–4.3)	ns
Liver intranuclear inclusions	2.3	(1.7–2.9)	4.1	(3.8–4.3)	<0.0001
Liver lipofuscin	2.8	(2.3–3.3)	2.2	(2.0–2.4)	0.036
Kidney anisokaryosis	1.1	(0.3–1.8)	4.2	(4.0–4.4)	<0.0001
Kidney tubular degeneration	2.8	(2.2–3.3)	2.0	(1.7–2.4)	0.043
Heart myocardial degeneration	1.9	(1.2–2.7)	2.0	(1.6–2.3)	ns
Brain vacuolization	3.0	(2.3–3.7)	1.8	(1.3–2.4)	0.014
Spinal cord vacuolization	3.1	(2.5–3.7)	2.2	(1.7–2.7)	0.032
Peripheral nerve vacuolization	2.8	(2.6–3.6)	2.9	(2.3–3.6)	ns
Femur bone marrow fatty infiltration[b]	1.2	(0.5–2.0)	3.3	(2.8–3.8)	0.0002
Testis tubular degeneration	2.2	(1.5–2.9)	4.7	(4.3–5.2)	0.0002

Note: End-of-life: moribund mice from life span cohorts. Combined results of male and female mice based on 10–35 mice per group, except for testis for which 10 and 7 males were analyzed per group.
ns, not significant.
[a]Mann–Whitney test (two-tailed) was used for all genotype and sex specific comparisons
[b]Statistical differences between sexes within genotypes were not found, except for the histopathology score of 'Femur bone marrow fatty infiltration' among *Ercc1*$^{-/\Delta 7}$ mice; males: 2.8 (2.2–3.5) and females: 3.8 (3.1–4.6), $p = 0.0403$. When analyzed by sex the histopathology score for 'Femur bone marrow fatty infiltration' was higher in both males ($p = 0.0060$) and females ($p = 0.0211$) in *Ercc1*$^{-/\Delta 7}$ mice compared to *Ercc1*$^{+/+}$ mice.

(Table 1 and Fig. 4E, F), already at 4 weeks of age and increasing with age. The effect was slightly more severe in females of both genotypes, which may be consistent with the slightly increased spleen weights in a number of aging females that was due to increased red pulp as a possible result of compensatory increased hematopoiesis. Apart from atrophy in the bone marrow, accelerated thymic involution was indicated by decreased thymus weight but apart from a smaller size, no further histological abnormalities were noted.

Testicular atrophy

The testes of *Ercc1*$^{-/\Delta 7}$ males were severely altered with atrophy of the germinal epithelium characterized by vacuolization of Sertoli cells, loss of germ cells, and occasional multinucleated remnants of spermatocytes (Table 1). Epididymis did not contain sperm, and the lesion was present from the earliest analyzed time point (4-week-old mice). The pattern resembles atrophy in aged wild-type testes, with the exception that in the latter there is more deposition of lipofuscin. However, since the onset is so early this lesion probably reflects a state of abiotrophy rather than senile atrophy. The testis has been described as a highly oxidative environment and tolerance for genetic abnormality is minimal in developing germ cells; hence, this lesion is observed frequently in genetically engineered mice. In *Ercc1*$^{-/-}$ mice, an increase in DNA instability was noted and testicular atrophy was thought to result from apoptosis in relation to oxidative stress (20).

Other lesions

A hunched spine posture (kyphosis) became apparent with advancing age in *Ercc1*$^{-/\Delta 7}$ mice (observational data, not shown). Histologically, in routine H&E stained sections there was infrequent and minimal degeneration of intervertebral discs in *Ercc1*$^{-/\Delta 7}$ mice, in contrast to an earlier report (21). Moreover, disc degeneration and herniation were much more severe in end-of-life *Ercc1*$^{+/+}$ than *Ercc1*$^{-/\Delta 7}$ mice (results not shown), indicating that these are not a consistent aging changes in *Ercc1*$^{-/\Delta 7}$ mice. Other changes were not observed with H&E stained sections, no other special staining techniques were used.

Mild vacuolization of cardiomyocytes was observed in Ercc1 deficient animals at an earlier age than wild-type, which may be indicative of a certain extent of myocardial degeneration.

The weakness and tremors, however, are more likely attributable to mild neurodegenerative changes including peripheral (sciatic) nerve vacuolization, and brain mass reduction in *Ercc1*$^{-/\Delta 7}$ mutants compared to wild-type. Although marked vacuolization of brain stem, striatum, and cerebellar medulla were occasionally observed in

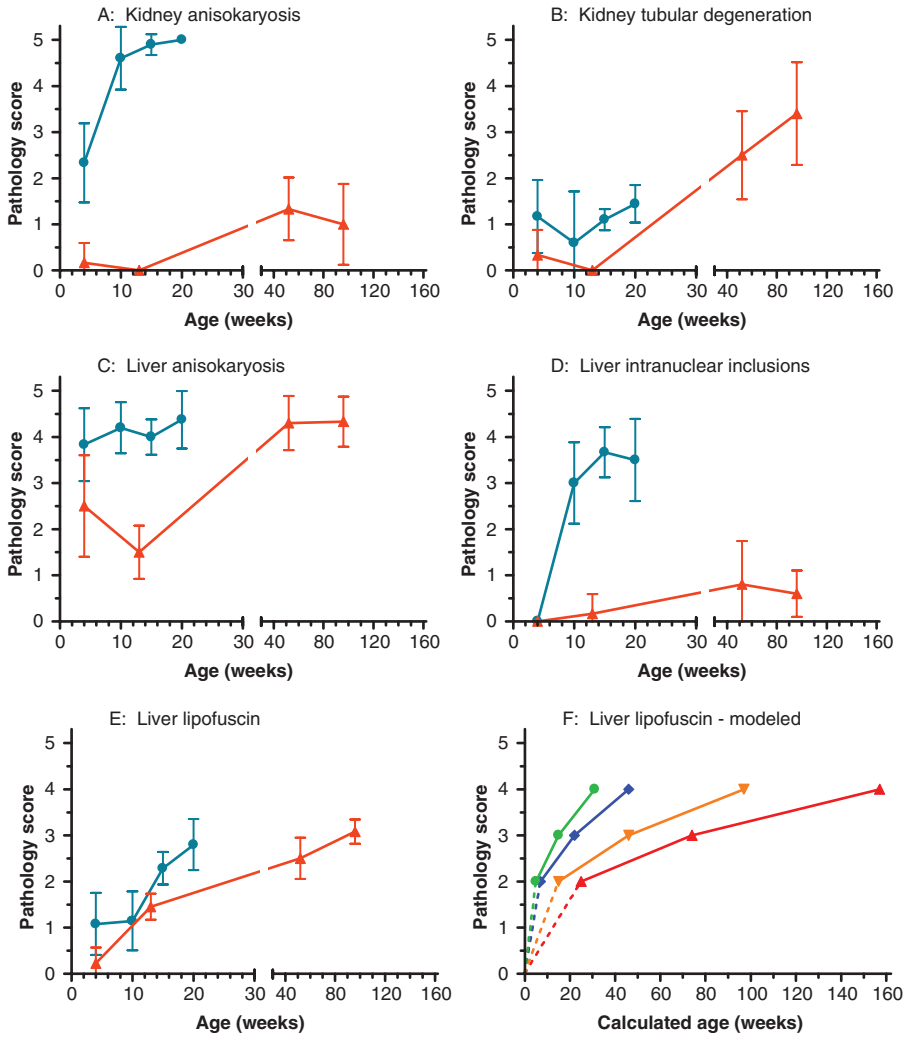

Fig. 3. Mean pathology scores of liver and kidney observations at cross-sectional age groups in *Ercc1*$^{-/\Delta 7}$ and *Ercc1*$^{+/+}$ mice. A: kidney anisokayosis, B: kidney tubular degeneration, C: liver anisokaryosis, D: liver intranuclear inclusions, and E: liver lipofuscin. Means are based on 5–31 organs per genotype and age group (males and females combined). The bars indicate the 95% confidence intervals. *Ercc1*$^{-/\Delta 7}$: blue dots; *Ercc1*$^{+/+}$: red triangles. F: Calculated age to reach lipofuscin pathology score for male and female *Ercc1*$^{-/\Delta 7}$ and *Ercc1*$^{+/+}$ mice. Modeled by PROAST, with exponential model 2: $y = a \exp(bx)$ as selected model, based on a total of 115 observations. Age at score 1 could not be calculated. *Ercc1*$^{-/\Delta 7}$ males: blue diamonds; *Ercc1*$^{-/\Delta 7}$ females: green dots; *Ercc1*$^{+/+}$ males: red triangles; and *Ercc1*$^{+/+}$ females: orange inverted triangles.

both genotypes, this lesion did not consistently correlate with behavioral abnormalities. However, we can not exclude that such vacuolization is a result of a formalin fixation artifact (22).

Immunosenescence

Lymphocyte subset distributions in thymocyte and splenocyte preparations were performed by flow cytometric analysis using antibodies directed at various cell surface markers. Lymphocyte preparations were made at two cross-sectional age groups for both genotypes: 4 and 14 weeks and an additional age group for *Ercc1*$^{+/+}$ at 96 weeks. Samples of five mice per sex, genotype and age group were analyzed. Thymocytes were stained for CD3, CD4 and CD8 to examine T-cell differentiation. Initially in the thymic cortex, stage II cells are characterized by relatively low CD3 expression and simultaneous CD4 and CD8 expression. During maturation into stage III cells CD3 expression increases and differentiation is marked by expression of either CD4 or CD8 (23). Fig. 5A plots the ratio of stage II to stage III T-cells for the different genotype/age groups. During development from 4 to 14 weeks of age *Ercc1*$^{+/+}$ mice have a relative increase in the stage II T-cell reservoir. The ratio at 96 weeks needs to be interpreted with care, as we obtained sufficient thymocytes from only one male and one female mouse at this age. As indicated by the thymus weights (Fig. 2J), thymic involution reduces the number of available cells at

Citation: Pathobiology of Aging & Age-related Diseases 2011, **1**: 7219 - DOI: 10.3402/pba.v1i0.7219

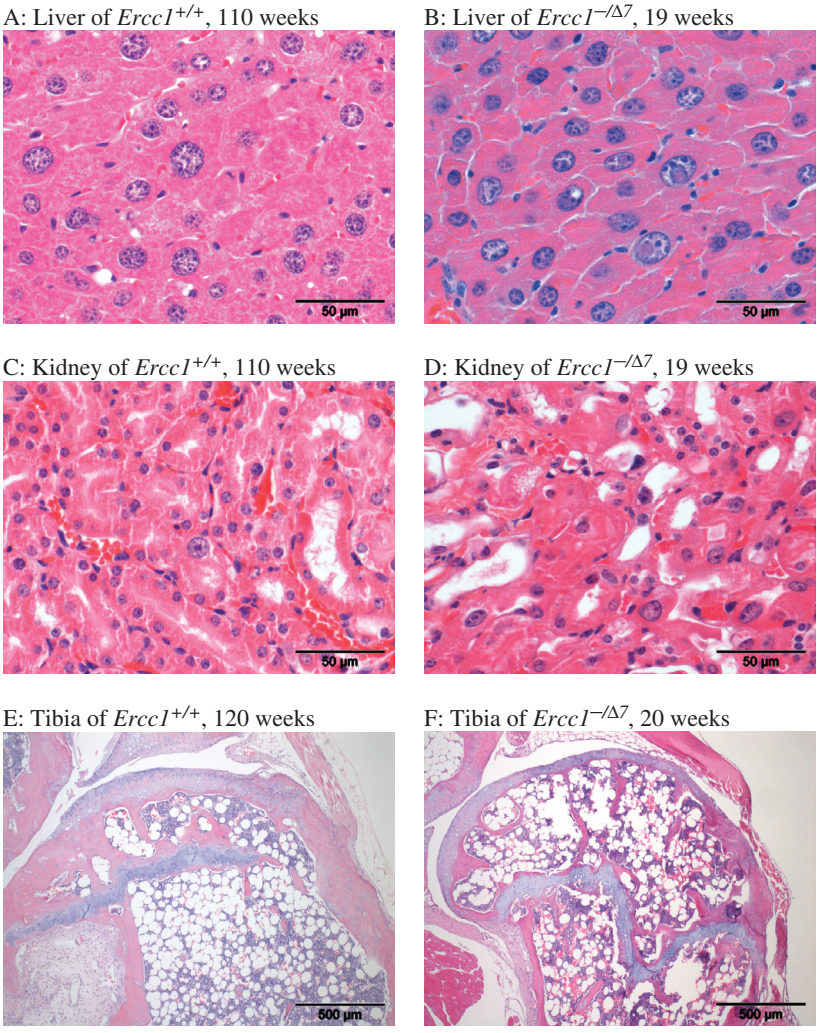

Fig. 4. Examples of histopathology in aging male $Ercc1^{+/+}$ and $Ercc1^{-/\Delta 7}$ mice. Liver of $Ercc1^{+/+}$, 110 weeks (A). Marked scattered anisokaryosis and karyomegaly (larger nuclei); note general absence of nuclear inclusions. Compare to liver of 19 weeks old $Ercc1^{-/\Delta 7}$ mutant (B): marked anisokaryosis and marked intranuclear cytoplasmic inclusions/invaginations. Kidney of 110 weeks old $Ercc1^{+/+}$ mouse shows rare karyomegaly (C) compared to 19 weeks old $Ercc1^{-/\Delta 7}$ mutant (D). Bone marrow fatty infiltration and atrophy is present in 120 weeks old $Ercc1^{+/+}$ (E) but even more pronounced in $Ercc1^{-/\Delta 7}$ mutant at 20 weeks (F).

old age. However, both the male and female sample suggest a decrease in the stage II/stage III ratio from 14 to 96 weeks of age. In $Ercc1^{-/\Delta 7}$ mice the ratio declines from 4 to 14 weeks to the level of that observed in the two 96 week old $Ercc1^{+/+}$ mice (Fig. 5A). The ratio of CD4 over CD8 differentiated mature T-cells showed no genotype difference within chronological age groups (results not shown).

CD45 positive splenocytes were subdivided into B-, T-, and natural killer (NK) cell fractions. The percentage of NK-cells in spleens of $Ercc1^{+/+}$ mice increased from 2.5% at 4 weeks to 5.5% at 14 weeks of age, followed by a decrease at age 96 weeks to 1.1% (Fig. 5B). In spleens of $Ercc1^{-/\Delta 7}$ mice NK-cells were already down to about 1.1% at 4 weeks of age, which was retained (males) or even further decreased (females) to 0.8% at 14 weeks of age (Fig. 5B). Age related changes in percentage of B- and T- cells showed no genotype differences within chronological age groups (data not shown).

Subsequently, the ratio of naïve (CD45RB positive) over memory (CD44) T-cells was determined for both CD4 and CD8 positive splenocytes (Fig. 5C, D). For CD4 and CD8 positive subclasses in $Ercc1^{+/+}$ mice, the ratio declined with advancing age over the three age groups, indicative of a relative reduction in naïve T-cells and increase in memory T-cells. $Ercc1^{-/\Delta 7}$ mice had similar naïve/memory CD4 positive T-cell ratios as $Ercc1^{+/+}$ mice at comparable chronological age groups (Fig. 5C). For CD8 positive T-cells the ratios were somewhat lower in $Ercc1^{-/\Delta 7}$ compared to $Ercc1^{+/+}$ mice at 4 weeks of age, but yielded similar values at 14 weeks of age (Fig. 5D).

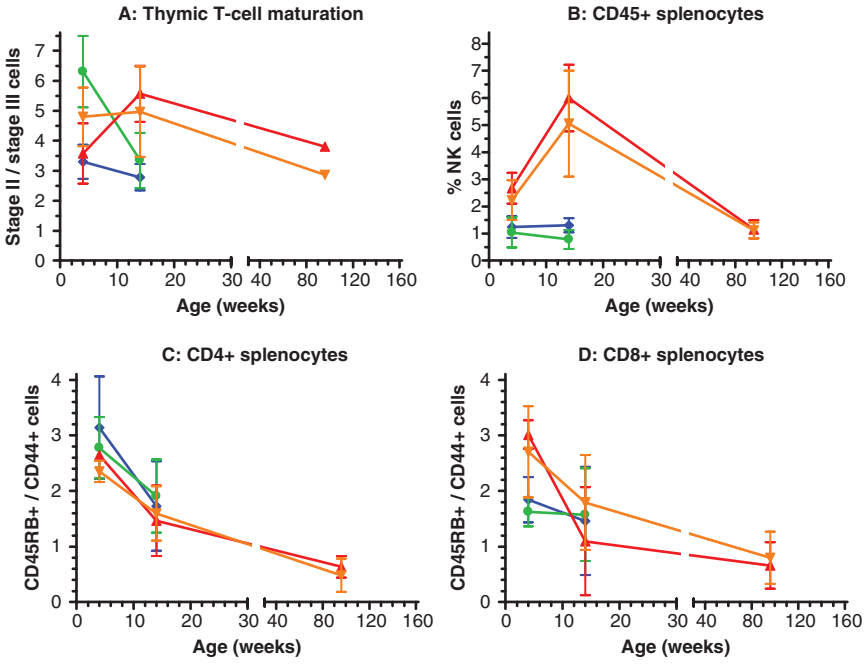

Fig. 5. Lymphocyte subset distributions in *Ercc1*$^{-/\Delta 7}$ and *Ercc1*$^{+/+}$ mice at cross-sectional age groups. A: T-cell distribution in the thymus as ratios of immature, stage II cells over mature stage III cells. B: Percentage of natural killer cells among CD45 positive splenocytes. C: Ratio of naïve over memory CD4 positive T-cells in spleen. D: Ratio of naïve over memory CD8 positive T-cells in spleen. All symbols display means of $n = 5$, except in graph A at 96 weeks, which represent a single individual value for each sex (see text for details). The error bars indicate standard deviations. *Ercc1*$^{-/\Delta 7}$ males: blue diamonds; *Ercc1*$^{-/\Delta 7}$ females: green dots; *Ercc1*$^{+/+}$ males: red triangles; and *Ercc1*$^{+/+}$ females: orange inverted triangles.

Discussion

In this report we present the first complete life span study of comprehensively characterized *Ercc1*$^{-/\Delta 7}$ mice and their wild-type sibling controls in an inbred genetic F1 hybrid background of C5BL6/J and FVB. We confirm the profoundly reduced life span and runted appearance of the Ercc1-deficient mice reported in earlier studies of more limited scope (6, 7, 12, 21). In addition, we extensively characterized the age-related changes in body weight and six internal organs and traced end-of-life histopathological observations back in cross-sectional age groups. We confirm some of the more severe progeroid symptoms reported previously for this same Ercc1 compromised model (7), or the closely related and even shorter lived full knockout mice (9, 11, 20). In addition, we found lipofuscin accumulation and myocardial degeneration as new progeroid pathological lesions in the *Ercc1*$^{-/\Delta 7}$ mouse model. Furthermore, using a small restricted number of cross-sectional age groups we identified some age-related changes of the immune system.

Taken together, a picture emerges of a segmental progeroid phenotype in *Ercc1*$^{-/\Delta 7}$ mice. Nearly all described aging-related changes also occur to some extent in DNA repair proficient wild-type mice. By comparing the aging-related changes over several cross-sectional age groups, one can differentiate between different aging rates of the individual endpoints. First, one can recognize processes that occur to the same extend when comparing chronological age groups between genotypes. These processes appear not to be Ercc1-related and, hence, could be classified as 'normal' aging. A detailed example of normal aging in this report is naïve T-cell depletion (Fig. 5C, D). Second, one can discern aging-related changes that are comparable between genotypes on a biological age scale, i.e. occur at the same point in their life span. Such changes could then be classified as 'accelerated' aging, resulting in about the same severity at end-of-life, exemplified by thymic involution (Fig. 2J), liver ansiokaryosis (Fig. 3C), hepatic lipofuscin accumulation (Fig. 3E, F), and T-cell maturation (Fig. 5A). And third, there are processes that are much more pronounced, even on a biological age scale, in Ercc1-deficient mice. Hence, we termed this class of endpoints such as liver intranuclear inclusions (Fig. 3D), kidney anisokaryosis (Fig. 3A), and NK-cell reduction (Fig. 5B) 'extreme' aging. These lesions also occur in aging wild-type animals though much milder. Of course, there are grey areas in this classification with endpoints falling between definitions. Nevertheless, we classified all endpoints in this report according to the description above in Table 2.

That the *Ercc1*$^{-/\Delta 7}$ progeroid phenotype is clearly segmental is shown by the normal aging classified end-

Citation: Pathobiology of Aging & Age-related Diseases 2011, **1**: 7219 - DOI: 10.3402/pba.v1i0.7219

points (Table 2), which follow the chronological age-related changes. Previously, in an aging cohort of another NER compromised mouse model, Xpd^{TTD}, we have shown that next to accelerated aging features, signs of ameliorated aging were found (4). Molecular characterization in various DNA repair deficient mouse models, including Ercc1 deficiency, indicate that these mice mount in part a similar expression profile as mouse models of extended life span, suggestive of an adaptive 'survival' response that could slow the aging rate (24, 25). Moreover, $Ercc1^{-/-}$ mice (10) and $Ercc1^{-/\Delta 7}$ mice (unpublished results) show signs of a suppressed somatotroph axis. Among the endpoints of this report we found no signs of reduced aging rates, except for the absence of tumors. A complicating factor here is the short life span of the $Ercc1^{-/\Delta 7}$ mice. Whereas the Xpd^{TTD} mutant mice studied previously had a medium life span of 93 weeks (4), $Ercc1^{-/\Delta 7}$ have a medium life span of only 20–21 weeks and a maximum of 29 weeks (Fig. 1A). Many aging related pathologies take more time than 30 weeks to become discernable in wild-type mice, let alone the reduction in incidence or severity. The absence of tumors in the wild-type cross-sectional cohort before 96 weeks of age suggests that the age of tumor onset is somewhere between 52 and 96 weeks. However, examples are known of mice deficient for genome maintenance genes that do show spontaneous tumor development within 30 weeks, e.g. p53 (26) and mice deficient in non-homolgous end joining (NHEJ) of double strand breaks (27). The NEHJ deficient mice in the same F1 C57BL/6-FVB hybrid background develop thymomas as young as 14 weeks (ongoing study, results not shown). Apparently Ercc1 is not involved in tumor repressing systems, or the unresolved lesions are toxic for the transformed cell.

The segmental progeroid phenotype of $Ercc1^{-/\Delta 7}$ mice has two potential practical advantages for aging research. First, the accelerated segmental nature of the aging phenotype could bring research focus on those specific endpoints, underlying causes, and consequences that would be more difficult to discern in wild-type mice that dilute these endpoints with the full aging spectrum. Second, short life span and the explicit aging aspects could make a suitable short-term intervention model for life span extension and reduction of aging related pathology. Both applications are currently being explored.

Table 2. Selective segmental progeria phenotype of $Ercc1^{-/\Delta 7}$ mice

Normal	Accelerated	Extreme
Brain vacuolization	Heart myocardial degeneration	Ataxia
Naïve T-cell depletion	Kidney tubular degeneration	Brain atrophy
Spinal cord vacuolization	Kyphosis	Femur bone marrow fatty infiltration
Tumors[a]	Liver anisokaryosis	Kidney anisokaryosis
	Liver lipofuscin	Liver intranuclear inclusions
	Peripheral nerve vacuolization	NK-cell reduction
	T-cell maturation	Spleen atrophy
	Thymic involution	Testis tubular degeneration

Note: Only endpoints studied in this report are included. Normal: comparable on chronological age scale; Accelerated: comparable on biological age scale; Extreme: more pronounced in $Ercc1^{-/\Delta 7}$ even on a biological age scale.
[a]No malignancies observed in $Ercc1^{-/\Delta 7}$ mice. $Ercc1^{+/+}$ mice at comparable chronological age do not show tumors either, but develop them later in life.

Acknowledgements

We thank Wout Slob for assistance with PROAST modeling. This research was funded by a grant from the National Institute for Public Health and the Environment and the Ministry of Health, Welfare and Sport of The Netherlands (S/340020) and the National Institutes of Health/National Institute of Aging (3PO1 AG017242).

Conflict of interest and funding

The authors have not received any funding or benefits from industry or elsewhere to conduct this study.

References

1. Hasty P, Campisi J, Hoeijmakers J, van Steeg H, Vijg J. Aging and genome maintenance: lessons from the mouse? Science 2003; 299: 1355–9.
2. Eriksson M, Brown WT, Gordon LB, Glynn MW, Singer J, Scott L., et al. Recurrent de novo point mutations in lamin A cause Hutchinson–Gilford progeria syndrome. Nature 2003; 423: 293–98.
3. Melis JP, Wijnhoven SWP, Beems RB, Roodbergen M, van den Berg J, Moon H, et al. Mouse models for xeroderma pigmentosum group A and group C show divergent cancer phenotypes. Cancer Res 2008; 68: 1347–53.
4. Wijnhoven SW, Beems RB, Roodbergen M, van den Berg J, Lohman PH, et al. Accelerated aging pathology in ad libitum fed Xpd(TTD) mice is accompanied by features suggestive of caloric restriction. DNA Repair (Amst) 2005; 4: 1314–24.
5. Niedernhofer LJ, Odijk H, Budzowska M, van Drunen E, Maas A, Theil AF, et al. The structure-specific endonuclease Ercc1-Xpf is required to resolve DNA interstrand cross-link-induced double-strand breaks. Mol Cell Biol 2004; 24: 5776–87.
6. Ahmad A, Robinson AR, Duensing A, van Drunen E, Beverloo HB, Weisberg DB, et al. ERCC1-XPF endonuclease facilitates DNA double-strand break repair. Mol Cell Biol 2008; 28: 5082–92.
7. Weeda G, Donker I, de Wit J, Morreau H, Janssens R, Vissers CJ, et al. Disruption of mouse ERCC1 results in a novel repair syndrome with growth failure, nuclear abnormalities and senescence. Curr Biol 1997; 7: 427–39.

8. Doig J, Anderson C, Lawrence NJ, Selfridge J, Brownstein DG, Melton DW. Mice with skin-specific DNA repair gene (Ercc1) inactivation are hypersensitive to ultraviolet irradiation-induced skin cancer and show more rapid actinic progression. Oncogene 2006; 25: 6229–38.
9. McWhir J, Selfridge J, Harrison DJ, Squires S, Melton DW. Mice with DNA repair gene (ERCC-1) deficiency have elevated levels of p53, liver nuclear abnormalities and die before weaning. Nat Genet 1993; 5: 217–24.
10. Niedernhofer LJ, Garinis GA, Raams A, Lalai AS, Robinson AR, Appeldoorn E, et al. A new progeroid syndrome reveals that genotoxic stress suppresses the somatotroph axis. Nature 2006; 444: 1038–43.
11. Prasher JM, Lalai AS, Heijmans-Antonissen C, Ploemacher RE, Hoeijmakers JHJ, Touw IP, et al. Reduced hematopoietic reserves in DNA interstrand crosslink repair-deficient Ercc1 −/− mice. EMBO J 2005; 24: 861–71.
12. Dollé ME, Busuttil RA, Garcia AM, Wijnhoven S, van Drunen E, Niedernhofer LJ, et al. Increased genomic instability is not a prerequisite for shortened lifespan in DNA repair deficient mice. Mutat Res 2006; 596: 22–35.
13. Dollé ME, Giese H, Hopkins CL, Martus HJ, Hausdorff JM, Vijg J. Rapid accumulation of genome rearrangements in liver but not in brain of old mice. Nat Genet 1997; 17: 431–4.
14. Nicklas W, Baneux P, Boot R, Decelle T, Deeny AA, Fumanelli M et al. Recommendations for the health monitoring of rodent and rabbit colonies in breeding and experimental units. Lab Anim 2002; 36: 20–42.
15. Terman A, Brunk UT. Lipofuscin. Int J Biochem Cell Biol 2004; 36: 1400–4.
16. Tonk EC, de Groot DM, Penninks AH, Waalkens-Berendsen ID, Wolterbeek AP, Slob W, et al. Developmental immunotoxicity of methylmercury: the relative sensitivity of developmental and immune parameters. Toxicol Sci 2010; 117: 325–35.
17. Slob W. Dose-response modeling of continuous endpoints. Toxicol Sci 2002; 66: 298–312.
18. de Waard MC, van der Pluijm I, Zuiderveen Borgesius N, Comley LH, Haasdijk ED, Rijksen Y, et al. Age-related motor neuron degeneration in DNA repair-deficient Ercc1 mice. Acta Neuropathol 2010; 120: 461–75.
19. Chipchase MD, O'Neill M, Melton DW. Characterization of premature liver polyploidy in DNA repair (Ercc1)-deficient mice. Hepatology 2003; 38: 958–66.
20. Hsia KT, Millar MR, King S, Selfridge J, Redhead NJ, Melton DW, et al. DNA repair gene Ercc1 is essential for normal spermatogenesis and oogenesis and for functional integrity of germ cell DNA in the mouse. Development 2003; 130: 369–78.
21. Vo N, Seo H-Y, Robinson A, Sowa G, Bentley D, Taylor L, et al. Accelerated aging of intervertebral discs in a mouse model of progeria. J Orthop Res 2010; 28: 1600–07.
22. Ward JM, Mahler JF, Maronpot RR. Pathology of genetically engineered mice. Ames, IA: Iowa State University Press; 2002.
23. Roitt I, Brostoff J, Male D. Immunology, 4th ed. London: Mosby; 1996.
24. Garinis GA, Uittenboogaard LM, Stachelscheid H, Fousteri M, van Ijcken W, Breit TM, et al. Persistent transcription-blocking DNA lesions trigger somatic growth attenuation associated with longevity. Nat Cell Biol 2009; 11: 604–15.
25. Schumacher B, van der Pluijm I, Moorhouse MJ, Kosteas T, Robinson AR, Suh Y, et al. Delayed and accelerated aging share common longevity assurance mechanisms. PLoS Genet 2008; 4: e1000161.
26. Donehower LA, Harvey M, Slagle BL, McArthur MJ, Montgomery CA, Butel JS, et al. Mice deficient for p53 are developmentally normal but susceptible to spontaneous tumours. Nature 1992; 356: 215–21.
27. Li GC, Ouyang H, Li X, Nagasawa H, Little JB, Chen DJ, et al. Ku70: a candidate tumor suppressor gene for murine T cell lymphoma. Mol Cell 1998; 2: 1–8.

***Martijn Dollé**
Laboratory of Health Protection Research (pb12)
National Institute of Public Health and the Environment
P.O. Box 1
3720 BA Bilthoven
The Netherlands
Tel: +31-30-2742011
Fax: +31-30-2744446
Email: Martijn.Dolle@rivm.nl

Citation: Pathobiology of Aging & Age-related Diseases 2011, **1**: 7219 - DOI: 10.3402/pba.v1i0.7219

Supplementary Table 1. Fate and animal numbers per initiated cohort

	Found dead	Moribund kills	Cross-sectional kill	Total
Life span cohorts:				
Ercc1$^{-/\Delta 7}$ males	8	23	not applicable	31
Ercc1$^{-/\Delta 7}$ females	10	19	not applicable	29
Ercc1$^{+/+}$ males	21	29	not applicable	50
Ercc1$^{+/+}$ females	10	41	not applicable	51
Cross-sectional cohorts:				
Ercc1$^{-/\Delta 7}$ males, 4 weeks	0	0	15	15
Ercc1$^{-/\Delta 7}$ males, 10 weeks	0	0	7	7
Ercc1$^{-/\Delta 7}$ males, 14 weeks	1	0	7	8
Ercc1$^{-/\Delta 7}$ males, 16 weeks	2	1	11	14
Ercc1$^{-/\Delta 7}$ males, 20 weeks	6	6	4	16
Ercc1$^{-/\Delta 7}$ females, 4 weeks	0	0	15	15
Ercc1$^{-/\Delta 7}$ females, 10 weeks	0	0	7	7
Ercc1$^{-/\Delta 7}$ females, 14 weeks	3	1	6	10
Ercc1$^{-/\Delta 7}$ females, 16 weeks	1	1	12	14
Ercc1$^{-/\Delta 7}$ females, 20 weeks	8	2	6	16
Ercc1$^{+/+}$ males, 4 weeks	0	0	6	6
Ercc1$^{+/+}$ males, 10 weeks	0	0	6	6
Ercc1$^{+/+}$ males, 13 weeks	0	0	15	15
Ercc1$^{+/+}$ males, 52 weeks	0	0	15	15
Ercc1$^{+/+}$ males, 96 weeks	4	1	12	17
Ercc1$^{+/+}$ females, 4 weeks	0	0	7	7
Ercc1$^{+/+}$ females, 10 weeks	0	0	7	7
Ercc1$^{+/+}$ females, 13 weeks	0	0	15	15
Ercc1$^{+/+}$ females, 52 weeks	0	0	16	16
Ercc1$^{+/+}$ females, 96 weeks	2	1	15	18

Supplementary Table 2. Organs and tissues collected at autopsy of moribund and cross-sectional sectioned animals

Material	Fixated in formaldehyde	Stored at −80°C
Abdomen:		
Adrenal glands	x	
Cervix and vagina (females)	x	
Coagulation gland (males)	x	
Epididymes (males)	x	
Gall bladder	x	
Kidneys	x	x
Liver	x	x
Large intestine (coe/col/rec)	x	x
Mammary gland	x	
Mesenteric lymph node	x	x
Pancreas	x	x
Preputial glands (males)	x	
Prostate (males)	x	
Seminal vesicles (males)	x	
Skin	x	x
Small intestine (duo/jej/ile)	x	x
Spleen	x	x
Stomach	x	
Testes (males)	x	x
Urinary bladder	x	
Uterus and ovaries (females)	x	
Chest cavity:		
Aorta	x	x
Heart	x	x
Larynx/thyroid gland/tongue	x	
Lungs	x	x
Esophagus	x	
Sternum	x	
Thymus	x	x
Trachea	x	
Head:		
Brains	x	x
Extraorbital lacrymal glands/ Zymbal glands	x	
Eyes	x	
Harderian gland	x	
Nose	x	
Pituitary gland (in skull)	x	
Salivary glands with manibular lymph nodes	x	
Other:		
Axillary lymph node (prop. and acces.)	x	x
Blood smear		
Femur (bone marrow)	x	x
Macroscopical changes, e.g. tumors	x	x
Pelvis and three vertebra	x	
Peripheral nerve (ischiadicus)	x	
Serum		x
Skeletal muscle, quadriceps	x	x
Spinal cord (*in situ*)	x	
Tail		x

Supplementary Table 2 (*Continued*)

Citation: Pathobiology of Aging & Age-related Diseases 2011, **1**: 7219 - DOI: 10.3402/pba.v1i0.7219